

Fluid Vesicles with Viscous Membranes in Shear Flow

Hiroshi Noguchi and Gerhard Gompper

Institut für Festkörperforschung, Forschungszentrum Jülich, 52425 Jülich, Germany

(Received 14 April 2004; published 13 December 2004)

The effect of membrane viscosity on the dynamics of vesicles in shear flow is studied. We present a new simulation technique, which combines three-dimensional multiparticle collision dynamics for the solvent with a dynamically triangulated membrane model. Vesicles are found to transit from steady tank treading to unsteady tumbling motion with increasing membrane viscosity. Depending on the reduced volume and membrane viscosity, shear can induce both discocyte-to-prolate and prolate-to-discocyte transformations. This behavior can be understood from a simplified model.

DOI: 10.1103/PhysRevLett.93.258102

PACS numbers: 87.16.Dg, 47.55.-t, 87.17.Aa

The dynamical behavior of lipid vesicles under shear flow is an important subject not only of fundamental research but also in medical applications [1]. For example, in microcirculation, the deformation of red blood cells reduces the flow resistance of microvessels. In diseases such as diabetes mellitus and sickle cell anemia, red blood cells have reduced deformability and often block microvascular flow. Although red blood cells do not have a nucleus and other intracellular organelles, they are more complex than lipid vesicles, since their plasma membrane has an attached spectrin network, which modifies its elastic and rheological properties.

The dynamical behavior of vesicles in shear flow has been studied experimentally [1,2], theoretically [3,4], and numerically [5–7]. The vesicle shape is determined by the competition of the curvature elasticity of the membrane, the constraints of constant volume V and constant surface area S , the viscoelasticity of the membrane, and the external hydrodynamic forces. One of the difficulties in theoretical studies of the hydrodynamic effects on the vesicle dynamics is the boundary condition for the embedding fluid on the vesicle surface, which changes its shape dynamically. In some previous studies, a fluid vesicle was therefore modeled as an ellipsoid with fixed shape [3]. More recently, the time evolution of the shape was studied numerically using a boundary integral method in three spatial dimensions [5] or an advected-field method in two spatial dimensions [6]. The red blood cell membrane has also been modeled as an elastic capsule of discocyte shape [7].

Two types of dynamics have been found in these studies, a steady state with a tank-treading motion of the membrane and a finite inclination angle with the flow direction, and an unsteady state with a tumbling (flipping) motion. A transition from tank treading to tumbling with an increasing viscosity of the internal fluid has been predicted for fluid vesicles with fixed ellipsoidal shape in three dimensions [3], and with the advected-field method in two dimensions [6]. When the shape is relaxed dynamically in three dimensions, all discocyte vesicles were surprisingly found to

transform into prolates in shear flow, even for the smallest shear rates studied [5].

In this Letter, we focus on the effect of the membrane viscosity on the dynamics of vesicles in shear flow. This is an important question, because the membrane of red blood cells, for example, becomes more viscous on aging [4,8] or in diabetes mellitus [9]. Experiments indicate that the energy dissipation in the membrane is larger than that inside a red blood cell [4]. Furthermore, it has been shown recently that vesicles can not only be made from lipid bilayers, but also from bilayers of block copolymers [10]. These “polymersomes” have been shown to have a membrane viscosity which is several orders of magnitude larger than for liposomes [11].

Several mesoscopic simulation techniques for fluid flow have been developed in recent years. We present here the first simulation studies for a combination of a mesoscopic model for the solvent and a coarse-grained, dynamically triangulated surface model for the membrane. This approach has four main advantages: (i) The membrane is described explicitly, so that their properties like the viscosity can be varied easily; (ii) thermal fluctuation of both the solvent and the membrane are fully and consistently taken into account; (iii) the method can easily be generalized to more complex flow geometries; and (iv) no numerical instabilities can occur.

We employ a particle-based hydrodynamics method [12–18] to simulate the solvent, which is called multiparticle collision dynamics (MPCD) [17,18] or stochastic rotation dynamics [14,15]. This method was applied, for example, to polymer dynamics [13,18]. The fluids in the interior and exterior of the vesicle are taken to be the same, in particular, to have the same viscosity η_0 .

As the MPCD model is described in detail in Refs. [12–15], we can be very brief in explaining the mesoscopic simulation technique. The solvent is described by N_s point-like particles of mass m_s moving in a rectangular box of size $L_x \times L_y \times L_z$. The algorithm consists of alternating streaming and collision steps. In the streaming step, the particles move ballistically and the position of each parti-

cle \mathbf{r}_i is updated according to $\mathbf{r}_i(t+h) = \mathbf{r}_i(t) + \mathbf{v}_i(t)h$, where \mathbf{v}_i is the velocity of particle i and h is the time interval between collisions. In the collision step, the particles are sorted into cubic cells of lattice constant a . The collision step consists of a stochastic rotation of the relative velocities of each particle in a cell, $\mathbf{v}_i^{(\text{new})}(t) = \mathbf{v}_{\text{cm}}(t) + \Omega(\varphi)(\mathbf{v}_i(t) - \mathbf{v}_{\text{cm}}(t))$, where \mathbf{v}_{cm} is the velocity of the center of mass of all particles in the cell. The matrix $\Omega(\varphi)$ rotates velocities by a fixed angle φ around an axis, which is chosen randomly for each cell. In our simulation, the angle $\varphi = \pi/2$ is employed. We apply a random-shift procedure [14] before each collision step to ensure Galilean invariance.

For the membrane, we employ a dynamically triangulated surface model [19], in which the membrane is described by N_{mb} vertices which are connected by tethers to form a triangular network. The vertices have excluded volume and mass m_{mb} . The shapes and fluctuations of the membrane are controlled by curvature elasticity with the energy, $H_{\text{cv}} = (\kappa/2) \int (C_1 + C_2)^2 dS$, where κ is the bending modulus, and C_1 and C_2 are the principal curvatures at each point of the membrane [20]. The curvature energy is discretized as described in Ref. [21]. To model the fluidity of the membrane, tethers can be flipped between the two possible diagonals of two adjacent triangles. These bond flips provide also a convenient way to vary the membrane viscosity η_{mb} , because it increases with decreasing bond-flip rate. We determine η_{mb} quantitatively from a simulation of a flat membrane in two-dimensional Poiseuille flow. In contrast to previous studies of dynamically triangulated surfaces, which were all done by Monte Carlo simulations, we introduce a smooth bond-interaction potential, which makes the model amenable for molecular dynamics simulations.

The solvent particles interact with the membrane in two ways. First, the membrane vertices are included in the MPCD collision procedure [13]. Second, the solvent particles are scattered elastically or via bounceback from membrane triangles. We use here the procedure suggested in Ref. [16] for a spherical particle.

To induce a shear flow, we employ Lees-Edwards boundary conditions [15,22], which give a linear flow profile $(v_x, v_y, v_z) = (\dot{\gamma}z, 0, 0)$ in the MPCD fluid. The particle density is set to $\rho = 10m_s/a^3$. For the system size $L_x = 50a$, $L_y = L_z = 30a$, this implies $N_s = 450\,000$. We have also done a few runs for smaller and larger system sizes to estimate finite-size effects [23]. In experimental conditions of red blood cells and liposomes, the Reynolds number $\text{Re} = \dot{\gamma}\rho R_0^2/\eta_0$ is very small ($\text{Re} \sim 10^{-3}$), where $R_0 = \sqrt{S/4\pi}$ is the effective vesicle radius. Therefore, we chose a short mean free path $h\sqrt{k_B T/m_s} = 0.025a$, where $k_B T$ is the thermal energy [18]. Then the viscosity of solvent fluid is $\eta_0 = 20.1\sqrt{m_s k_B T}/a^2$ [15]. We use $\kappa = 20k_B T$, $N_{\text{mb}} = 500$, and $m_{\text{mb}} = 10m_s$. The volume V and surface area $S = 405a^2$ of a vesicle are kept

constant to about 1% accuracy. With these parameters, we obtain a Reynolds number $\text{Re} \approx 0.1$. The results are conveniently expressed in terms of dimensionless variables: the reduced volume $V^* = V/(4\pi R_0^3/3)$, the intrinsic time scale $\tau = \eta_0 R_0^3/\kappa$, the reduced shear rate $\dot{\gamma}^* = \dot{\gamma}\tau$, and the relative membrane viscosity $\eta_{\text{mb}}^* = \eta_{\text{mb}}/\eta_0 R_0$. Details of the numerical scheme will be published elsewhere [23].

At $\eta_{\text{mb}}^* = 0$, simulated vesicles exhibit tank-treading motion for all investigated reduced volumes in the range $0.59 \leq V^* \leq 0.97$. We calculate the average inclination angles $\langle\theta\rangle$, and find them to agree very well with those obtained by the boundary integral method [5,24].

With increasing membrane viscosity η_{mb}^* , the inclination angle θ decreases, as shown in Fig. 1. The qualitative features of the simulation data are reproduced very well by the theory of Keller and Skalak (KS) [3,4]. Note that there are no adjustable parameters. Because of the approximations in the KS theory, an agreement on a quantitative level cannot be expected: (i) an ellipsoidal shape is assumed, which only mimics the real shapes of vesicles, (ii) the flow on the surface of the droplet is not locally area conserving, as it must be for an incompressible membrane, and (iii) thermal fluctuations are ignored in the theory, but are present in the simulations. In the KS theory, the vesicle transits from tank treading to tumbling motion when the angle θ reaches 0. In contrast, we observe tumbling intermittently to occur already for nonzero $\langle\theta\rangle$, since our simulation includes thermal fluctuation. For example, the vesicle with $V^* = 0.78$ starts tumbling at $\eta_{\text{mb}}^* = 1.22$.

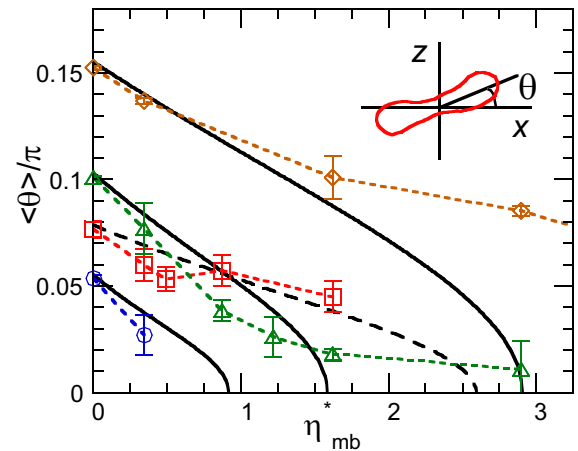


FIG. 1 (color online). Dependence of the average inclination angle $\langle\theta\rangle$ ($-\pi/2 \leq \theta < \pi/2$) on the membrane viscosity η_{mb}^* for reduced shear rate $\dot{\gamma}^* = 0.92$ and various reduced volumes V^* . The error bars are estimated from three independent runs [24]. Squares and circles represent discocyte and prolate vesicles at $V^* = 0.59$, respectively. Triangles and diamonds represent prolate vesicles at $V^* = 0.78$ and $V^* = 0.91$, where the prolate is the only stable shape. The solid lines and broken line are calculated by KS theory with prolate ($V^* = 0.59, 0.78$, and 0.91) and oblate ellipsoids ($V^* = 0.59$), respectively.

This intermittent tumbling smoothes out the decrease in $\langle\theta\rangle$ around the transition point; see Fig. 1.

We now focus on the case $V^* = 0.59$. At this reduced volume, the discocyte shape is stable and the prolate and stomatocyte shapes are metastable in the absence of shear flow. Figure 2 shows the free-energy F as a function of the asphericity α , calculated with a version of the generalized-ensemble Monte Carlo method [25]. The asphericity $\alpha = (1/2)[(\lambda_1 - \lambda_2)^2 + (\lambda_2 - \lambda_3)^2 + (\lambda_3 - \lambda_1)^2]/(\lambda_1 + \lambda_2 + \lambda_3)^2$, with the eigenvalues $\lambda_1 \leq \lambda_2 \leq \lambda_3$ of the moment-of-inertia tensor, is a convenient measure to distinguish oblate and prolate shapes, where $\alpha = 0$ for spheres, $\alpha = 1$ for thin rods, and $\alpha = 0.25$ for thin discs [26]. The free-energy minima agree well with previous $T = 0$ calculations [27]. However, thermal fluctuations and nonaxisymmetric shapes are important to obtain $F(\alpha)$. The shear flow changes this stability. A dynamical phase diagram is shown in Fig. 3. For membrane viscosity $\eta_{mb}^* = 0$ and shear rates $\dot{\gamma}^* \gtrsim 1.6$, the discocyte state is found to be destabilized and to transform into a prolate, in agreement with the results of Ref. [5]. However, for smaller shear rates of $\dot{\gamma}^* \lesssim 1.0$, the discocyte vesicle retains its shape. Speculations about shear to be a singular perturbation [5] can therefore be ruled out.

The inclination angle θ of prolates decreases faster than that of discocytes with increasing η_{mb}^* ; see Fig. 1. At a large membrane viscosity of $\eta_{mb}^* = 1.62$, the prolate enters the tumbling phase, while the discocyte remains in the tank-treading phase. The reason is that the discocyte has a flat dimple region and is less affected by the membrane viscosity than the prolate. Remarkably, for small shear rates, the (metastable) prolate starts tumbling, but after a π or 2π rotation, transforms into a tank-treading discocyte, see Fig. 4. Only for larger shear rates, the tumbling continues—accompanied by shape oscillations between prolate and discocyte. At intermediate membrane viscosities, $\eta_{mb}^* = 0.49$ or 0.87 , and shear rate $\dot{\gamma}^* = 0.92$, the prolate transforms into a discocyte after tank-treading motion for a time of $(70 \pm 40)\tau$ or $(40 \pm 20)\tau$ by thermal fluctuation, respectively. For larger shear rates, the tumbling continues intermittently.

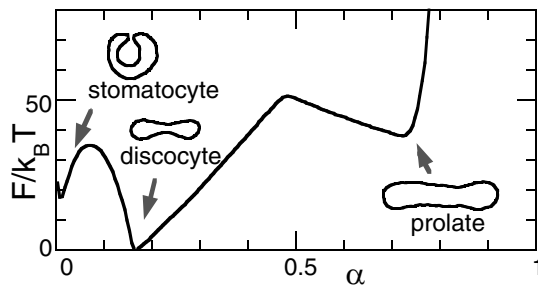


FIG. 2. Free-energy profile $F(\alpha)$ of the asphericity α for $V^* = 0.59$ in the absence of shear flow. Cross sections of snapshots of stable (discocyte) and metastable (prolate and stomatocyte) shapes are also shown.

KS theory [3,4] explains the η_{mb}^* dependence of the stability of tank treading (compare Fig. 1), but cannot be applied to describe the dynamics, including morphological changes. We therefore suggest a simple phenomenological model, which is defined by the equations

$$\zeta_\alpha \dot{\alpha} = -\kappa^{-1} \partial F / \partial \alpha + A \dot{\gamma}^* \sin(2\theta) \quad (1)$$

$$\dot{\theta} = 0.5 \dot{\gamma}^* \{-1 + B(\alpha) \cos(2\theta)\}. \quad (2)$$

The force $\partial F / \partial \alpha$ is calculated from the free-energy $F(\alpha)$ of Fig. 2. The second term of Eq. (1) is the deformation force due to the shear flow. Its θ dependence can be deduced from the shape equations of Ref. [5], while the amplitude is assumed to be independent of the asphericity α (to leading order). Equation (2) is adopted from KS theory [3,4]. Here, B is a constant which depends on viscosities and ellipsoid shape. For $B > 1$, a steady angle $\theta = 0.5 \arccos(1/B)$ exists and tank-treading motion occurs, while for $B < 1$, there is no stable angle and tumbling motion occurs. In our case, the vesicle shape can be time dependent, so that B is no longer constant. For simplicity, we assume a linear dependence of B on the asphericity, $B(\alpha) = B_0 - B_1 \alpha$. To obtain tank-treading discocytes and tumbling prolate, we need $B(0.2) > 1$ and $B(0.7) < 1$, respectively. Then, Eqs. (1) and (2) reproduce the simulated dynamics very well; see Fig. 4. The vesicle is found, for example, to relax after some tumbling to a stable, tank-treading discocyte state at $\dot{\gamma}^* = 1.84$, and to relax to a limit-cycle oscillation between discocyte and prolate at $\dot{\gamma}^* = 2.76$.

The smooth crossover from tank treading to tumbling in Fig. 1 for $V^* = 0.78$ can also be obtained from this simplified model when Eqs. (1) and (2) are extended to include stochastic terms [23].

The simplified model also gives some insight into the shape transformations with shear. Shear flow increases the elongation of a vesicle in the tank-treading regime $0 < \theta < \pi/2$ (where $\dot{\gamma}^* \sin(2\theta) > 0$), but reduces the elongation for $-\pi/2 < \theta < 0$ (where $\dot{\gamma}^* \sin(2\theta) < 0$) during tumbling.

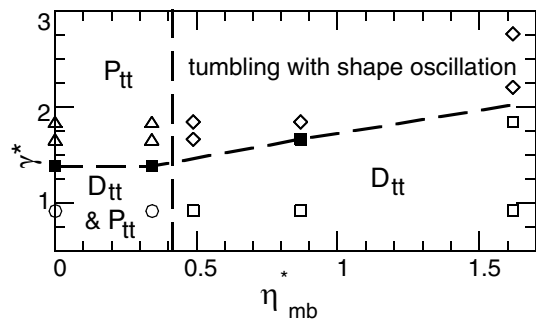


FIG. 3. Dynamical phase diagram of vesicle in shear flow, with $V^* = 0.59$. “D” and “P” denote discocyte and prolate shapes, respectively. “tt” indicates tank treading. Symbols show simulated parameter values. The broken lines are guides to the eye.

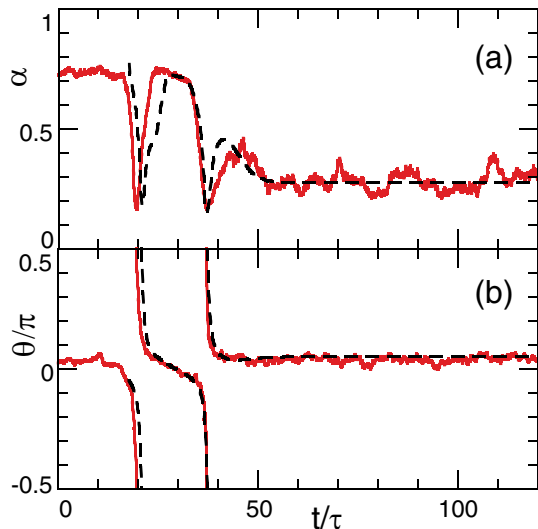


FIG. 4 (color online). Time development of (a) asphericity α and (b) inclination angle θ , for $V^* = 0.59$, $\eta_{mb}^* = 1.62$, and $\dot{\gamma}^* = 1.84$. The broken lines are obtained from Eqs. (1) and (2) with $\zeta_\alpha = 100$, $A = 15$, and $B(\alpha) = 1.1 - 0.18\alpha$.

The force in the former case induces the discocyte-to-prolate transformation; in the latter case the prolate-to-discocyte transformation. With increasing membrane viscosity η_{mb}^* , the inclination angle θ of the tank-treading discocyte decreases, and larger shear rates $\dot{\gamma}^*$ are necessary to generate the required elongational forces to induce a discocyte-to-prolate transition; compare Fig. 3.

It is also interesting to compare the effect of membrane viscosity η_{mb} and internal viscosity η_{in} . In both cases, an increase of the viscosity induces a decrease of the inclination angle θ and a transition from tank treading to tumbling. However, the effect of internal viscosity η_{in} is less dependent on the vesicle morphology. KS theory [3] shows that with increasing η_{in} , the tank-treading phase of oblate vesicles is destabilized a little faster (at $\eta_{in}/\eta_0 = 2.8$) than that of prolates (at $\eta_{in}/\eta_0 = 3.2$) for $\eta_{mb}^* = 0$. Thus, only a sufficiently high membrane viscosity η_{mb}^* can induce the transformation from tumbling prolate to tank-treading discocyte.

The membrane viscosity of human red blood cells is estimated from the analysis of the tank-treading motion to be $\eta_{mb} = 10^{-7}$ N s/m [4], while a micropipette recovery-time technique gives $\eta_{mb} = 10^{-6}$ N s/m [8]. When the viscosity of the external fluid is set to the same value of the intracellular fluid, $\eta_0 = 10^{-2}$ Pa s, and $R_0 = 3.3 \mu\text{m}$, the relative membrane viscosity is found to be in the range $\eta_{mb}^* = 1 \dots 10$. Thus, the effect of this membrane viscosity is sufficiently large (compare Fig. 1) to strongly affect the dynamics of erythrocytes. The viscoelasticity of membrane can be changed by varying the chemical composition of the solvent [1]. It is difficult to separate the effects of viscosity and elasticity, however. On the other hand, polymersomes seem to be very well suited for experimental studies of this

effect, since their membrane viscosity can be changed over a wide range by varying the polymer chain length.

In summary, we have shown that the MPCD method in combination with dynamically triangulated surfaces is a powerful tool to study vesicle hydrodynamics. The deformations of viscoelastic vesicles and other flow geometries will be interesting subjects in further studies.

We would like to thank N. Kikuchi (Oxford), A. Lamura (Bari), and R. G. Winkler for helpful discussions. H. N.'s stay at FZJ was supported by Research Abroad of the Japan Society for the Promotion of Science (JSPS).

-
- [1] S. Chien, Annual Review of Physiology **49**, 177 (1987).
 - [2] T.M. Fischer, M. Stöhr-Liesen, and H. Schmid-Schönbein, Science **202**, 894 (1978).
 - [3] S.R. Keller and R. Skalak, J. Fluid Mech. **120**, 27 (1982).
 - [4] R. Tran-Son-Tay, S.P. Suter, and P.R. Rao, Biophys. J. **46**, 65 (1984).
 - [5] M. Kraus, W. Wintz, U. Seifert, and R. Lipowsky, Phys. Rev. Lett. **77**, 3685 (1996).
 - [6] J. Beaucourt *et al.*, Phys. Rev. E **69**, 011906 (2004).
 - [7] C. Pozrikidis, Ann. Biomed. Eng. **31**, 1194 (2003).
 - [8] G.B. Nash and H.J. Meiselman, Biophys. J. **43**, 63 (1983).
 - [9] K. Tsukada, E. Sekizuka, C. Oshio, and H. Minamitani, Microvasc. Res. **61**, 231 (2001).
 - [10] B.M. Discher *et al.*, Science **284**, 1143 (1999).
 - [11] R. Dimova *et al.*, Eur. Phys. J. E **7**, 241 (2002).
 - [12] A. Malevanets and R. Kapral, J. Chem. Phys. **110**, 8605 (1999).
 - [13] A. Malevanets and J.M. Yeomans, Europhys. Lett. **52**, 231 (2000).
 - [14] T. Ihle and D.M. Kroll, Phys. Rev. E **63**, 020201(R) (2001).
 - [15] N. Kikuchi, C.M. Pooley, J.F. Ryder, and J.M. Yeomans, J. Chem. Phys. **119**, 6388 (2003).
 - [16] N. Kikuchi, Ph. D. thesis, University of Oxford 2003.
 - [17] A. Lamura, G. Gompper, T. Ihle, and D. M. Kroll, Europhys. Lett. **56**, 319 (2001).
 - [18] M. Ripoll, K. Mussawisade, R. G. Winkler, and G. Gompper, Europhys. Lett. **68**, 106 (2004).
 - [19] G. Gompper and D.M. Kroll, J. Phys. Condens. Matter **9**, 8795 (1997).
 - [20] W. Helfrich, Z. Naturforsch. **28C**, 693 (1973).
 - [21] G. Gompper and D.M. Kroll, J. Phys. I (France) **6**, 1305 (1996).
 - [22] M.P. Allen and D.J. Tildesley, *Computer Simulation of Liquids* (Clarendon, Oxford, 1987).
 - [23] H. Noguchi and G. Gompper to be published.
 - [24] Finite-size effects are small, but increase with decreasing V^* . For $V^* = 0.59$ and $\eta_{mb} = 0$, we find that the inclination angle is underestimated by about 10%. This is comparable to our statistical error bars.
 - [25] B. A. Berg, H. Noguchi, and Y. Okamoto, Phys. Rev. E **68**, 036126 (2003).
 - [26] J. Rudnick and G. Gaspari, J. Phys. A **19**, L191 (1986).
 - [27] U. Seifert, K. Berndl, and R. Lipowsky, Phys. Rev. A **44**, 1182 (1991).